PROBABILISTIC SEISMIC DEMAND AND FRAGILITY OF FAULT-CROSSING BRIDGES USING GAUSSIAN PROCESS REGRESSION

Libo Chen [1], Zhaohui Zhang [2]

[1] *Associate Professor, College of Civil Engineering, Fuzhou University, lbchen@fzu.edu.cn*
[2] *Master Student, College of Civil Engineering, Fuzhou University, 2539216192@qq.com*

Abstract

To accurately evaluate the seismic performance of fault-crossing simply supported bridges under non-uniform seismic excitation, a vector-valued probabilistic seismic demand and fragility analysis framework based on Gaussian process regression (GPR) is proposed to effectively quantify the coupled effects of inertial force and differential displacement. To address the scarcity of near-fault recorded data, a hybrid simulation method combining fault geometry with physical and stochastic processes is first employed to generate a nonstationary cross-fault ground-motion field. On this basis, a two-stage feature selection method is used to identify peak ground velocity (PGV) and peak relative ground displacement (PRGD) as the joint intensity measures, and a nonparametric probabilistic seismic demand model (PSDM) is established. The results show that GPR can effectively represent the complex nonlinear relationship between the intensity measures and structural responses. The influence of differential displacement on component fragility is evident: an increase in PRGD reduces the PGV threshold corresponding to a specific damage state, and this trend is particularly pronounced in displacement-sensitive components such as bearings. Compared with the conventional single-intensity-measure approach, the proposed framework can characterize structural demand under fault-crossing scenarios more comprehensively, thus providing rigorous quantitative support for seismic design optimization and risk assessment of bridges.

Keywords: *fault-crossing bridge; Gaussian process regression; PSDM; seismic fragility*

1. Introduction

Earthquakes can severely damage bridge structures and disrupt post-earthquake transportation and emergency response. They often cause damage to bridge structures, thereby affecting post-earthquake traffic recovery and emergency rescue. With the continuous development of transportation infrastructure in strong-earthquake regions of southwestern China, some bridge projects can no longer completely avoid active faults, and the seismic safety of fault-crossing bridges has become an increasingly prominent issue. Unlike ordinary bridges, fault-crossing bridges are affected not only by near-fault velocity pulses, rupture directivity, and hanging-wall effects, but also by the combined action of fault permanent displacement and non-uniform seismic excitation on the two sides of the fault. As a result, such structures are more susceptible to large deformation and damage [1-4]. Therefore, seismic demand and fragility analysis of fault-crossing bridges is of great significance for understanding their mechanical characteristics and damage patterns.

Considerable research has been conducted on the seismic behavior of near-fault and fault-crossing bridges. Yang [1], Jia Hongyu[5], and others systematically reviewed the damage characteristics and research progress of fault-crossing bridges, and pointed out that fault displacement, pulse effects, and structural configuration are important factors affecting bridge damage. Goel, Chopra, and others [6-8] proposed simplified methods for seismic response analysis of fault-crossing bridges at an early stage, laying the foundation for subsequent studies. Thereafter, through quasi-static tests, shaking table tests, and nonlinear time-history analysis, other researchers further revealed the effects of factors such as the fault crossing angle, fault intersection location, and permanent ground displacement on bridge response and failure modes [9-11]. In the area of probabilistic seismic demand analysis of bridges, Mackie et al. [12] established a probabilistic seismic demand model, providing a methodological basis for demand analysis and fragility assessment. For the seismic fragility of near-fault bridges, Zhong et al. [13] pointed out that pulse effects can significantly increase the damage probability of components in simply supported bridges. Existing studies have shown that near-fault and fault-crossing ground motions can aggravate bridge damage, and that fault displacement, velocity pulses, and non-uniform excitation have important effects on structural response.

Overall, existing studies have mainly focused on the response characteristics, critical loading conditions, and controlling parameters of fault-crossing bridges, whereas relatively less attention has been paid to the statistical relationship between seismic intensity measures and engineering demand parameters. In particular, for fault-crossing bridges, a single intensity measure can hardly capture both the velocity-pulse effect and the relative displacement across the fault, resulting in limited ability to distinguish risk under different fault-crossing scenarios. Meanwhile, conventional probabilistic seismic demand models are mostly based on log-linear forms, which remain insufficient for describing complex nonlinear relationships. Previous studies have shown that Gaussian process regression has good applicability in dealing with nonlinear mapping relationships and uncertainty quantification [14-16].

Therefore, this study takes a fault-crossing simply supported bridge in southwestern China as the research object, uses a broadband hybrid method to generate non-uniform cross-fault ground motions on both sides of the bridge site, establishes a vector-valued probabilistic seismic demand model based on GPR, and further conducts seismic fragility analysis on this basis, so as to provide a reference for the seismic performance assessment of fault-crossing bridges.

2. Bridge Modeling and Cross-Fault Ground-Motion Simulation

2.1 Construction of the Bridge Finite Element Model

A three-span prestressed concrete simply supported T-beam bridge located in southwestern China was selected as the case-study bridge. The bridge span arrangement is 3×30 m. The superstructure of each span consists of five prestressed concrete T-beams. Each girder is 2.10 m wide and 2.50 m deep, and the concrete strength grade is C40. The substructure adopts double-column circular piers. The heights of Pier 2 and Pier 3 are both 12 m, and the pier column diameter is 1.40 m. The cap beam is 8.0 m long, with a section size of 1.60 m×1.40 m. Two transverse rows of plate rubber bearings, with a total of 10 bearings, are arranged at the top of the cap beam, and 0.50 m×0.50 m seismic shear keys are provided on both sides. A tie beam with a section size of 1.1 m×1.3 m is arranged at the middle height of the double-column pier. The concrete strength grade of the pier columns, cap beam, and tie beam is C30. A schematic of the relative positions of the fault and the bridge is shown in Fig. 1.

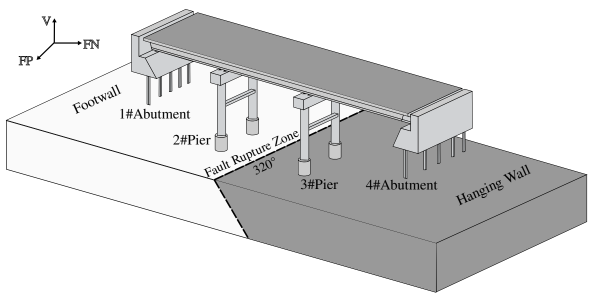

Fig. 1 – Schematic of the relative positions of the fault and the bridge

The finite element model of the bridge was established in OpenSees. According to previous damage investigations of girder bridges and related research findings, bridge damage is mainly concentrated in the bearings and substructure, whereas the girder components generally remain in the linear elastic range during earthquakes. The girders were modeled using three-dimensional elastic beam elements, and the corresponding mass was assigned to each element. As the primary nonlinear load-carrying components, the piers were modeled using force-based beam-column elements, and the sections were discretized into fibers. Each pier section was divided into three parts, namely confined concrete, cover concrete, and longitudinal reinforcement. The concrete was modeled using the Concrete02 material, and the reinforcing steel was modeled using the Hysteretic material. As transverse members connecting the double-column piers, the cap beam and tie beam were modeled using nonlinear beam-column elements, and the nodes at the tops of the pier columns and the corresponding cap beam nodes were treated as rigidly connected.

For the pounding effects between adjacent girders and between the girders and the abutments, zero-length Gap elements were arranged at the expansion-joint locations. Plate rubber bearings were used in the bridge, and were equivalently modeled in the finite element model by a bilinear restoring-force relationship. The abutments were modeled using a simplified method. Rigid arms were arranged at the girder ends of the side spans, where bearing elements, pounding gap elements, and wing-wall interaction elements were connected in parallel. In addition, zero-length elements were arranged at the bottoms of the abutments to simulate the combined effects of passive earth pressure behind the abutments and foundation restraint. The backfill soil behind the abutments was modeled using the Hyperbolic Gap material, and the combined action was realized through a Parallel Material assembly. The foundation restraint was treated using an equivalent boundary-spring method. Six-degree-of-freedom springs were assigned at the pier bases to simulate the foundation constraint effect, and the equivalent stiffness parameters in each direction were calculated by the *m* method. A schematic of the bridge finite element model is shown in Fig. 2. In the nonlinear time-history analysis of the bridge, three-component ground motions were input into the bridge using non-uniform excitation.

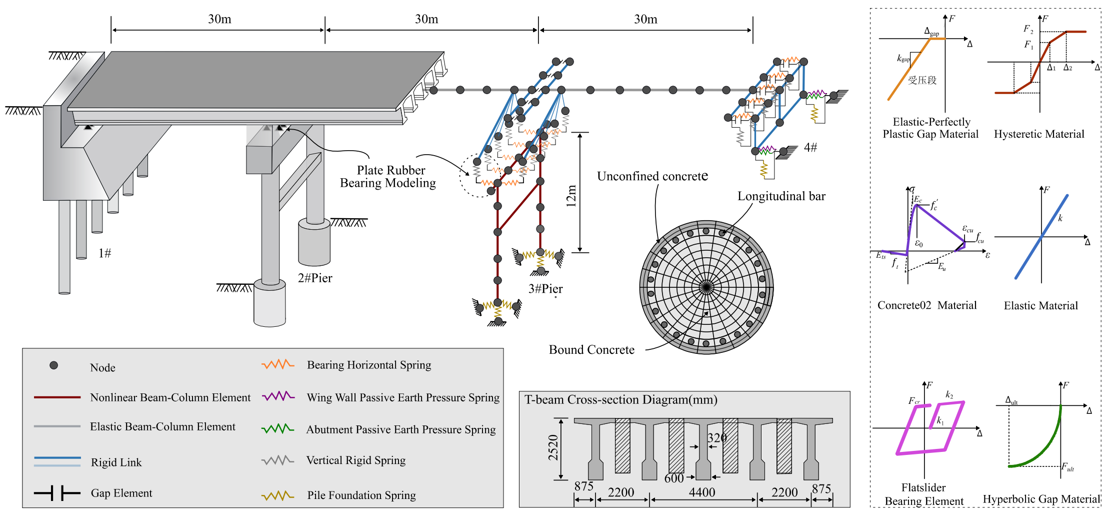

Fig. 2 – Finite element model of the bridge

2.2 Ground-Motion Simulation

In fault-crossing bridge projects, the bridge site spans the two sides of a fault, and the seismic input exhibits pronounced spatial variability and near-fault characteristics. However, among the recorded ground motions available in existing domestic and international databases, there are relatively few near-fault records that can be directly used for the analysis of fault-crossing bridges, and these records are insufficient to meet the needs of seismic analysis for engineering structures in such regions. To construct seismic input consistent with fault-crossing scenarios, it is therefore necessary to use near-fault ground-motion simulation methods. The hybrid method combines the capability of physics-based approaches to describe low-frequency permanent-displacement components with the advantage of stochastic approaches in simulating high-frequency components, and is suitable for constructing non-uniform seismic input for fault-crossing conditions. In this study, the broadband hybrid method previously validated by the authors is adopted to generate ground motions on both sides of the bridge site. Existing validation results show that the mean logarithmic residuals of the RotD50 pseudo-acceleration response spectra of the simulated ground motions within the target period range satisfy the preset threshold, indicating that they can meet the requirements of subsequent structural analysis under non-uniform excitation [17].

3. Seismic Intensity Measures and Engineering Demand Parameters

3.1 Determination of Seismic Parameters

In this study, cross-fault ground motions are simulated using a branch fault of the Zemuhe seismic fault zone in the near-fault region of southwestern China as the engineering background. The study area is located at the southern end of the Zemuhe fault zone. The fault is an active strike-slip fault and has remained highly active since the Late Pleistocene. Geological investigations indicate that its maximum earthquake magnitude is 6.0-6.9. Based on previous studies of fault ground-motion simulation and considering engineering safety, the maximum potential magnitude is taken as 7.0. This branch fault has a length of about 40 km and a width of about 17 km. The fault parameters required for the simulation are listed in Table 1.

Table 1 – Parameters of the Zemuhe Fault

Fault parameter	**Value**	**Fault parameter**	**Value**
Fault length	40 km	Hypocenter along-strike position	0 km
Fault width	17 km	Hypocenter down-dip position	8.5 km
Fault center latitude	27.01°	Corner frequency	1 Hz
Fault center longitude	102.76°	Shear-wave velocity	612 m/s
Fault strike	320°	Spectral attenuation parameter	0.063

The number and diversity of ground-motion samples are key factors in improving the predictive accuracy of the probabilistic seismic demand model and can provide a more reliable basis for the seismic performance assessment of bridge structures. Based on the site conditions at the bridge location, the broadband hybrid method is adopted to simulate ground motions. Considering the potential seismic capacity of the controlling fault at the bridge site, the maximum potential magnitude is taken as 7.0. To represent increasing source sizes in a scenario-based analysis, three representative magnitudes (Mw 5.9, 6.1, and 6.4) were considered. These magnitudes are used for parametric comparison correspond to code-defined frequent, design-level, and rare earthquakes, which established through site-specific seismic hazard analysis. Although the Zemuhe fault is used as the geographical background, the adopted dip-rake combinations are treated as generalized parametric scenarios rather than a site-specific source model. Near-fault ground motions and the resulting structural responses are relatively sensitive to source mechanisms and fault geometric parameters. Uncertainty in source parameters may alter the spectral characteristics and pulse effects of ground motions, thereby increasing the dispersion of bridge seismic demand. Therefore, key source parameters such as fault dip angle and rake angle are discretized and combined to construct rupture scenarios: the dip angle is taken as 30°, 50°, and 70°, and the rake angle is taken as -90°, -45°, 0°, 45°, and 90°, resulting in a total of 45 scenarios. To further represent the randomness and uncertainty of ground motions, 30 simulations are performed for each scenario, and a total of more than 1350 ground-motion samples are finally obtained for subsequent analysis.

3.2 Candidate Set of Intensity Measures and Two-Stage Screening

The selection of seismic intensity measures (IMs) directly affects the predictive accuracy and dispersion control of the probabilistic seismic demand model. For fault-crossing bridges, the seismic input includes not only the near-fault velocity-pulse effect, but may also involve significant relative displacement input caused by the difference in ground motion on the two sides of the fault. Therefore, the use of conventional single-point intensity measures alone is insufficient to comprehensively characterize the features of cross-fault ground motions. It is thus necessary to introduce differential-motion measures in addition to amplitude-based measures, so as to construct an IM system more suitable for the analysis of fault-crossing bridges.

Based on the above considerations, a candidate set of seismic intensity measures is established in this study, including the single-point intensity measures PGA, PGV, and spectral acceleration $S_a(T_1)$, as well as the cross-fault differential-motion measures PRGD, PRGV, and PDGD. The single-point measures are used to characterize the amplitude level of ground motion at a single observation point, whereas the differential-motion measures are used to quantify the difference in site motion across the fault. To ensure consistency with the subsequent analysis under three-component non-uniform seismic excitation, all the above measures are calculated separately in the three orthogonal components, namely fault-parallel (FP), fault-normal (FN), and vertical (V). According to the spatial relationship between the bridge and the fault, Piers 2 and 3, located on the two sides of the fault, are selected as the corresponding observation points. Let the displacement and velocity time histories of Piers 2 and 3 in direction $d$be denoted by $u_{(2,d)}(t)$, $u_{(3,d)}(t)$, $v_{(2,d)}(t)$, and $v_{(3,d)}(t)$, respectively. The cross-fault differential-motion intensity measures are then defined in Eq. (1) - (3).

$$PRGD = \max_t \left| u_{2,d}(t) - u_{3,d}(t) \right|$$

\(1\)

¿
¿

$$PRGV = \max_t \left| v_{2,d}(t) - v_{3,d}(t) \right|$$

\(2\)

$$PDGD=\left|u_{2,d}\left(t_e\right)-u_{3,d}\left(t_e\right)\right| \tag{3}$$

where PRGD denotes the peak relative ground displacement difference between the two sides of the fault over the entire duration, and is used to characterize the maximum differential-displacement effect in cross-fault input; PRGV denotes the peak relative ground velocity difference; and PDGD denotes the permanent relative displacement difference between the two sides after the end of the earthquake, and is used to describe the residual differential-displacement input.

After the candidate measures are determined, a two-stage feature-screening strategy is adopted to avoid directly specifying the IMs based only on experience. In the first stage, elastic net regression is used for preliminary screening. By simultaneously introducing the L_1 and L_2 regularization terms, elastic net can perform variable shrinkage and selection while handling multicollinearity. It is therefore suitable for removing redundant variables from the candidate IM set and identifying candidate features that make stable contributions to the engineering demand parameters (EDPs) [18-20]. In the second stage, Gaussian process regression (GPR) models are constructed based on the preliminarily screened results, and SHAP and permutation importance (PI) analyses are further combined to evaluate the contribution of each measure to EDP prediction. Since the GPR model can capture the complex nonlinear relationship between IMs and EDPs, this stage enables a more reliable assessment of feature importance within a nonlinear modeling framework. It should be noted that the specific modeling principle of GPR is presented in Section 4.1; here, it is used only as a feature-selection tool.

The results indicate that, although the important measures vary to some extent across different EDPs, PGV and PRGD consistently exhibit relatively high and stable contributions in the prediction of all types of EDPs. Among them, PRGD has a more pronounced influence on the curvature ductility demand at the pier base, indicating that the plastic response of the piers is more sensitive to the relative displacement difference across the fault. In the prediction of bearing shear deformation, both PGV and PRGD show high importance, indicating that the bearing response is jointly controlled by the near-fault velocity-pulse effect and the differential-displacement effect. Considering the screening stability, physical significance, and the requirements of subsequent fragility modeling, PGV and PRGD are finally selected as the vector-valued intensity measures in this study, while a single-IM model based on PGV is used as the benchmark for subsequent probabilistic seismic demand and fragility analyses. PGV and PRGD are calculated and statistically analyzed separately in the two horizontal components, namely FP and FN. Together, they are used to represent the near-fault velocity-pulse input and the cross-fault differential-displacement effect, thereby providing a more targeted intensity measure for subsequent seismic demand modeling.

3.3 Selection of Engineering Demand Parameters

Engineering demand parameters are quantitative indicators used to characterize structural seismic response and damage level, and their selection is directly related to the reliability of seismic performance assessment results. As the primary load-carrying components of the bridge substructure, piers are prone to enter the inelastic range and form plastic hinge regions under earthquake action, and thus constitute key components controlling the seismic performance of the structure. Compared with the overall displacement ductility index, the curvature ductility index can more directly reflect the extent of nonlinear development and the damage level at critical sections. Accordingly, the curvature ductility factor at the pier base section is selected in this study as the engineering demand parameter for the piers, in order to characterize their nonlinear response under earthquake action.

Bearings are key force-transferring components connecting the superstructure and substructure, and their seismic performance has an important influence on the overall mechanical state of the bridge. The bridge considered in this study adopts plate rubber bearings, whose seismic response is dominated by shear deformation. Excessive shear deformation may lead to functional failure. Based on existing experimental results and engineering experience, the maximum shear deformation of the bearings during the earthquake is selected as the engineering demand parameter in this study. This parameter is further evaluated together with the total thickness of the rubber layers for capacity assessment, so as to determine the bearing damage state.

4. Establishment of the Probabilistic Seismic Demand Model

A Gaussian process is a stochastic process defined over a continuous input space and can be used to construct the probabilistic mapping between seismic intensity measures (IMs) and engineering demand parameters (EDPs). In view of the pronounced nonlinearity and dispersion in the seismic response of the bridge considered in this study under strong earthquakes, Gaussian process regression (GPR) is adopted to establish the probabilistic seismic demand model. This method is a nonparametric Bayesian regression model, which can directly characterize the nonlinear relationship between IMs and EDPs without prescribing a functional form in advance, while simultaneously providing the predictive mean and an uncertainty measure.

4.1 Gaussian Process Regression Model

Compared with the conventional linear probabilistic seismic demand model, the GPR model can represent the nonlinear relationship between structural seismic response and ground-motion intensity more flexibly. Its regression form is given in Eq. (4).

$$y=f(x)+\varepsilon,\varepsilon\sim N(0,\sigma_n^2)$$

\(4\)

where $f(x)$ follows a Gaussian process prior, i.e., $f(x)\sim GP\left(0,k^f(x,x')\right)$, and ε is independently and identically distributed Gaussian noise. Given the training samples $D=\{X,y\}$, the predictive distribution at any input $x^{¿}$remains Gaussian, and the predictive mean and variance are expressed in Eq. (5) and Eq. (6), respectively.

$$\mu(x_{¿})=K_{x_{¿},X}\left(K_{X,X}+\sigma_n^2 I\right)^{-1}y$$

\(5\)

$$\sigma^2(x_{\text{¿}}) = k_f(x_{\text{¿}}, x_{\text{¿}}) - K_{x_{\text{¿}},X}\left(K_{X,X} + \sigma_n^2 I\right)^{-1} K_{X,x_{\text{¿}}}$$
（6）

The kernel function is given in Eq. (7).

$$k_f(x, x') = \sigma_f^2 \exp\left[\frac{-1}{2}\sum_{j=1}^{d}\left(\frac{x_j - x'_j}{l_j}\right)^2\right]$$
\(7\)

¿
¿

The covariance matrix $K_{X,X}$ is constructed from the noise-free kernel $k_f(\cdot,\cdot)$, while the observation noise is introduced separately through the term $\sigma_n^2 I$ in the predictive equations.

In this study, a total of 1350 samples of non-uniform ground motions are used as input, and probabilistic seismic demand models are established separately in the fault-normal (FN) and fault-parallel (FP) directions. For the input intensity measures, a single-IM model based on PGV is first constructed to characterize the basic trend of engineering demand with increasing ground-motion intensity. On this basis, PRGD is further introduced and combined with PGV to form vector-valued intensity measures, and a two-dimensional demand model is established to jointly reflect the effects of the velocity-pulse effect and the differential-displacement effect on structural response. The model output is the logarithmic value of the engineering demand parameter in the corresponding direction, which is used for subsequent seismic demand analysis and fragility assessment.

4.2 Probabilistic Seismic Demand Models

To compare the fitting performance of the single-IM model for different EDPs, Fig. 3 presents the results of the single-IM probabilistic seismic demand models established by GPR. The scatter points represent the engineering demand parameters corresponding to the ground-motion samples, the solid lines represent the GPR predictive means, and the shaded bands denote the 95% prediction intervals. All types of EDPs generally increase with PGV and exhibit nonlinear characteristics. Noticeable scatter remains at similar PGV levels. The wider prediction bands in the high-intensity range indicate larger predictive uncertainty in regions with stronger nonlinearity and fewer samples, rather than directly implying intensity-dependent demand dispersion. These results suggest that, when PGV alone is used as the single intensity measure, its ability to explain demand dispersion remains limited.

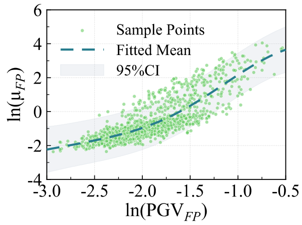

(a) Transverse curvature ductility factor at the pier base

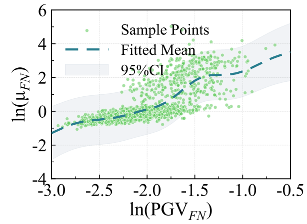

(b) Longitudinal curvature ductility factor at the pier base

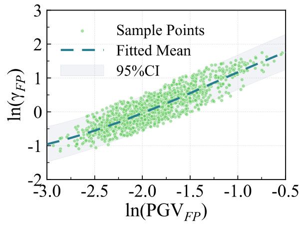

(c) Transverse bearing shear deformation

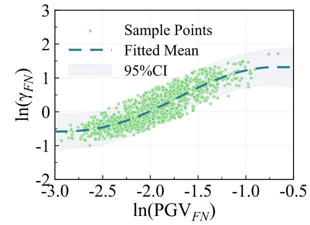

(d) Longitudinal bearing shear deformation

Fig. 3 – Single-IM probabilistic seismic demand models

To examine the variation of the demand surface in the two-dimensional intensity space after introducing PRGD, Fig. 4 presents the results of the vector-valued model. The colored surfaces denote the predictive mean surfaces, and the scatter points denote the sample distribution. Compared with the single-IM model, the vector-valued model characterizes the variation of EDPs in both the PGV and PRGD dimensions, allowing the demand differences under similar PGV conditions to be distinguished along the PRGD dimension. Overall, all types of EDPs increase with increasing PGV and PRGD, although the sensitivities differ among components and directions. The pier ductility indices are more sensitive to PRGD, whereas the bearing shear deformations are influenced by both PGV and PRGD, with a more pronounced increase observed in the region with high PGV and high PRGD. These results indicate that the introduction of vector-valued intensity measures helps improve the ability of the demand model to characterize differences in seismic input.

Compared with the single-IM PGV model, the vector-valued model yields smaller values of AIC, BIC, and leave-one-out cross-validation (LOO-CV) score for all four EDPs. After introducing PRGD, the demand models for all types of EDPs exhibit better fitting performance and stronger sample discrimination capability, indicating that vector-valued intensity measures are more suitable for characterizing demand differences under fault-crossing input.

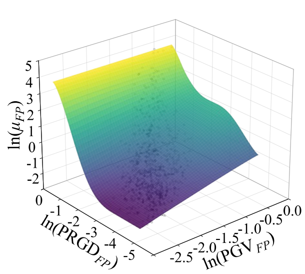

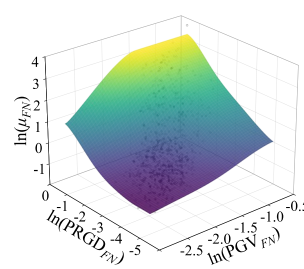

(a) Transverse curvature ductility factor at the pier base

(b) Longitudinal curvature ductility factor at the pier base

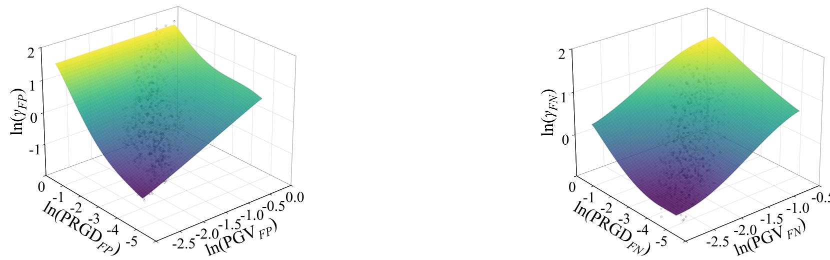

(c) Transverse bearing shear deformation

(d) Longitudinal bearing shear deformation

Fig. 4 – Probabilistic seismic demand models based on vector-valued intensity measures

5. Seismic Fragility Analysis of the Bridge

5.1 Fragility Modeling

Based on the Gaussian process-based probabilistic seismic demand models established in the preceding sections, seismic fragility models for bridge components can be further constructed. A fragility function is used to describe the conditional probability that a structure or component reaches or exceeds a certain damage state under a given level of seismic intensity [21]. In this study, both the seismic demand and the seismic capacity of components are assumed to follow lognormal distributions, and the component fragility functions are established accordingly.

The fragility function can be expressed as Eq. (8).

$$P_f = P\left(D \geq C \mid \Im\right) \tag{8}$$

When both demand and capacity follow lognormal distributions, Eq. (9) is obtained.

$$P\left[D \geq C \vee \Im\right] = \Phi\left(\frac{\ln\left(\widehat{D}\right) - \ln\left(\widehat{C}\right)}{\sqrt{\beta_{D \vee \Im}^2 + \beta_C^2}}\right) \tag{9}$$

where $\widehat{D}$ and $\widehat{C}$ are the median values of the component seismic demand and structural capacity, respectively; $\beta_{D|\Im}$ is the logarithmic standard deviation of demand; β_C is the logarithmic standard deviation of capacity; and $\Phi(\cdot)$ is the standard normal cumulative distribution function.

In the fragility analysis, the median demand is obtained as $\widehat{D}(\Im) = \exp\left[\mu_{\ln EDP}(\Im)\right]$, where $\mu_{\ln EDP}(\Im)$ is the predictive mean of the GPR model. A homoscedastic approximation is adopted in this study, and the demand dispersion $\beta_{D\vee\mathfrak{I}}$ is taken as the residual standard deviation of $\ln(EDP)$ estimated from the training data. Considering the specific characteristics of fault-crossing bridges, fragility functions are constructed separately using scalar PGV and the vector-valued intensity measures (PGV, PRGD) as the intensity measures, and the exceedance probabilities under different damage states are calculated by the above equations.

5.2 Definition of Damage States for Bridge Components

Considering that piers and bearings are the key components most vulnerable to seismic damage in the bridge system, the curvature ductility factor at the pier base and the bearing shear deformation are selected in this study as the damage indices for the two component types, respectively, and the component damage states are defined according to existing studies and code recommendations. For the piers, curvature ductility thresholds corresponding to the HAZUS damage states are adopted. For the plate rubber bearings, shear deformation is used as the damage quantification index, and 100%, 150%, 200%, and 250% are taken as the threshold values between adjacent damage states. To avoid the crossing of fragility curves caused by using different dispersion parameters for different damage states, $\beta_C$is uniformly taken as 0.30 in this study, following the assumptions of Nielson [22] and Porter [23]. The damage-state thresholds for each component are listed in Table 2.

Table 2 – Definition of Damage States for Bridge Components

Damage state	**Curvature ductility at pier base**	**Bearing shear deformation**
No damage	$\mu \leq 1.0$	$\gamma_a < 100\%$
Slight damage	$1.0 \leq \mu \leq 5.11$	$100\% \leq \gamma_a < 150\%$
Moderate damage	$5.11 \leq \mu \leq 7.5$	$150\% \leq \gamma_a < 200\%$
Extensive damage	$7.5 \leq \mu \leq 9$	$200\% \leq \gamma_a < 250\%$
Complete damage	$\mu \geq 9$	$\gamma_a \geq 250\%$

5.3 Seismic Fragility of the Bridge

5.3.1 Fragility Analysis Based on Vector-Valued Intensity Measures

Based on the vector-valued probabilistic seismic demand models established in the preceding sections and the defined component damage states, the fragility surfaces and conditional fragility curves of bridge components under different combinations of PGV and PRGD can be obtained. Owing to space limitations, only the transverse results of the piers and bearings are presented and discussed herein to illustrate the influence of cross-fault differential displacement on component damage probability.

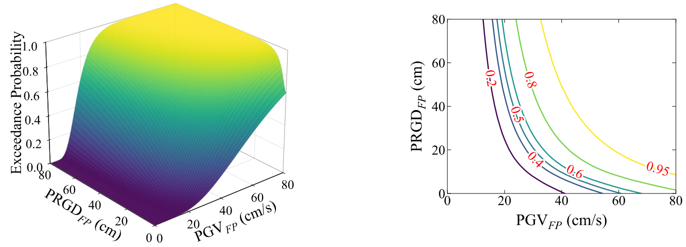

(a) Fragility surface

(b) Contour plot

Fig. 5 – Exceedance probability of transverse pier response at DS_2

Fig. 5 presents the fragility surface and contour plot of the transverse pier response at damage state DS_2. It can be seen that, with the increase in PGV and PRGD, the exceedance probability of the transverse pier reaching this damage state gradually increases, indicating that both the velocity-based ground-motion intensity and the differential displacement contribute to a higher probability of pier damage. The contours generally exhibit a downward-curving pattern toward the right, indicating that, at the same exceedance probability level, a larger PRGD corresponds to a smaller PGV required to reach this damage state. This suggests that the transverse pier damage is affected not only by PGV, but also by the cross-fault differential displacement. Therefore, the vector-valued intensity measures composed of PGV and PRGD can better reflect the damage risk under different differential-displacement conditions.

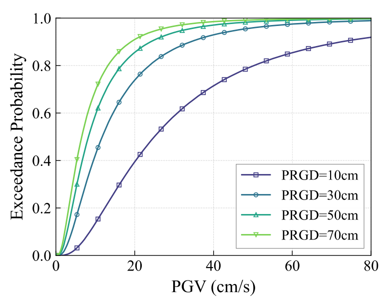

Fig. 6 – Sensitivity of the exceedance probability of transverse bearing response at DS_3 to PRGD

Fig. 6 shows the conditional fragility curves of the transverse bearing response at damage state DS_3 under different PRGD levels. The fragility curves under different PRGD conditions are clearly distinguishable, and they shift to the left as PRGD increases, indicating that the transverse bearings are relatively sensitive to differential displacement. When PRGD increases from 10 cm to 70 cm, the median PGV corresponding to this damage state for the transverse bearing decreases from 24.98 cm/s to 6.55 cm/s, representing a reduction of 73.78%. This indicates that, as the differential displacement increases, the velocity-based intensity level required for the bearing to enter this damage state decreases, and the transverse bearing response is relatively sensitive to changes in PRGD.

5.3.2 Comparative Analysis of Fragility Based on Single and Vector-Valued Intensity Measures

To compare the difference in risk discrimination capability between the single-IM and vector-valued IM approaches, Fig. 7 presents a comparison of the conditional fragility curves of the transverse pier response under different damage states. The curve of the single-IM model lies within the range formed by the conditional fragility curves of the vector-valued model under different PRGD levels, indicating that the fragility relationship established using PGV alone reflects the overall risk under different differential-displacement conditions. As PRGD increases from 5 cm to 40 cm and 80 cm, the curves of the vector-valued model shift toward the lower-PGV region as a whole, indicating that the PGV required to reach the same exceedance probability decreases as the differential displacement increases. This shows that the single-IM model cannot distinguish the risk differences under different differential-displacement scenarios, whereas the vector-valued model can reflect the variation in component fragility under fault-crossing input conditions.

Taking the median PGV corresponding to a 50% exceedance probability as an example, when PRGD=5 cm, the results of the single-IM model and the vector-valued model are relatively close. When PRGD increases to 40 cm and 80 cm, the median PGV predicted by the vector-valued model becomes lower than that of the single-IM model. Taking DS_3 as an example, the median PGV of the transverse pier decreases from 38.96 cm/s in the single-IM model to 29.52 cm/s and 22.22 cm/s in the vector-valued model. This indicates that, when PRGD is neglected, the single-IM model overestimates the ground-motion intensity required for the component to reach a given damage probability, thereby underestimating the actual risk under medium- to high-differential-displacement conditions.

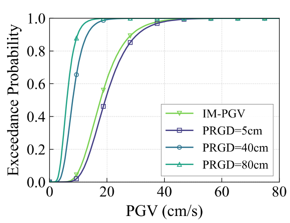

(a) Slight damage

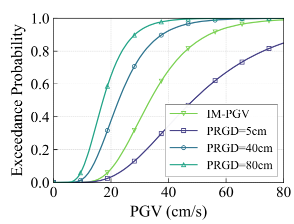

(b) Moderate damage

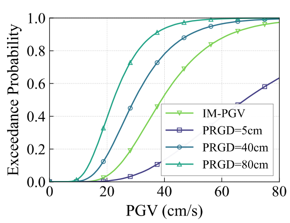

(c) Extensive damage

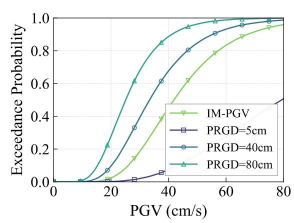

(d) Complete damage

Fig. 7 – Comparison of fragility curves of the transverse pier based on single and vector-valued intensity measures

6. Conclusions

This study considered a fault-crossing simply supported bridge in southwestern China, generated non-uniform cross-fault ground motions on both sides of the bridge site, and established a probabilistic seismic demand and fragility analysis framework based on Gaussian process regression (GPR). The main conclusions are as follows:

(1) Non-uniform cross-fault ground-motion samples on both sides of the bridge site were generated using the broadband hybrid method. The response-spectrum validation results indicate that the generated samples can be used for the analysis of fault-crossing bridges under non-uniform excitation.

(2) Through preliminary screening using elastic net regression and interpretability analysis based on GPR, PGV and PRGD were identified from the candidate measures as the preferred intensity measures. Compared with the single-IM model based on PGV, the vector-valued demand model is better able to distinguish response differences under similar PGV levels.

(3) An increase in PRGD shifts the conditional fragility curves of critical components toward lower PGV levels, with the bearings showing higher sensitivity. Compared with the scalar PGV-based model, the vector-valued IM model better distinguishes the component-level damage risk under different differential-displacement conditions.

7. References

[1] Yang S, Mavroeidis G P. Bridges crossing fault rupture zones: A review[J]. Soil Dynamics and Earthquake Engineering, 2018, 113: 545-571.

[2] 宗周红, 林元铮, 林津, 等. 跨断层地震动及其对桥梁结构影响研究进展 [J]. 中国公路学报,2023,36(01):80-96.

[3] 王东升, 郭迅, 孙治国, 等. 汶川大地震公路桥梁震害初步调查[J]. 地震工程与工程振动, 2009, 29(3): 84-94.

[4] 庄卫林, 刘振宇, 蒋劲松. 汶川大地震公路桥梁震害分析及对策[J]. 岩石力学与工程学报, 2009, 28(7): 1377-1387.

[5] 贾宏宇, 杨健, 郑史雄, 等. 跨断层桥梁抗震综述[J]. 西南交通大学学报, 2021, 56(05):1075-1093.

[6] Goel R K, Chopra A K. Linear analysis of ordinary bridges crossing fault-rupture zones[J]. Journal of Bridge Engineering, 2009, 14(3): 203-215.

[7] Goel R K, Chopra A K. Nonlinear analysis of ordinary bridges crossing fault-rupture zones[J]. Journal of Bridge Engineering, 2009, 14(3): 216-224.

[8] Goel R, Qu B, Tures J, et al. Validation of fault rupture-response spectrum analysis method for curved bridges crossing strike-slip fault rupture zones[J]. Journal of Bridge Engineering, 2014, 19(5): 06014002.

[9] Murono Y, Miroku A, Konno K. Experimental study on mechanism of fault-induced damage of bridges[C]//Proc. of the 13th World Conference on Earthquake Engineering. 2004.

[10] Saiidi M S, Vosooghi A, Choi H, et al. Shake table studies and analysis of a two-span RC bridge model subjected to a fault rupture[J]. Journal of Bridge Engineering, 2014, 19(8): A4014003.

[11] Lin Y, Zong Z, Bi K, Hao H, Lin J, Chen Y. Experimental and numerical studies of the seismic behavior of a steel-concrete composite rigid-frame bridge subjected to the surface rupture at a thrust fault[J]. Engineering Structures, 2020, 205:110105.

[12] Mackie K R, Stojadinović B. Performance-based seismic bridge design for damage and loss limit states[J]. Earthquake engineering & structural dynamics, 2007, 36(13): 1953-1971.

[13] Zhong J, Jiang L, Pang Y, et al. Near-fault seismic risk assessment of simply supported bridges[J]. Earthquake Spectra, 2020, 36(4): 1645-1669.

[14] Box G E P, Cox D R. An analysis of transformations[J]. Journal of the Royal Statistical Society Series B: Statistical Methodology, 1964, 26(2): 211-243.

[15] Guo J, Gao K, Dang X, et al. Seismic fragility assessment for highway bridges incorporating multi-level shape memory alloy cable dampers[J]. Engineering Structures, 2023, 287: 116172.

[16] 何志昆, 刘光斌, 赵曦晶, 等. 高斯过程回归方法综述[J]. 控制与决策, 2013, 28(8): 1121-1129.

[17] 陈力波, 陈何煜, 栗怀广, 等. 毗邻断层桥梁概率性地震需求模型及地震易损性研究[J]. 土木工程学报, 2025, 58(12): 90-102.

[18] Zou H, Hastie T. Regularization and variable selection via the elastic net[J]. Journal of the Royal Statistical Society Series B: Statistical Methodology, 2005, 67(2): 301-320.

[19] Hoerl A E, Kennard R W. Ridge regression: Biased estimation for nonorthogonal problems[J]. Technometrics, 1970, 12(1): 55-67.

[20] Tibshirani R. Regression shrinkage and selection via the lasso[J]. Journal of the Royal Statistical Society Series B: Statistical Methodology, 1996, 58(1): 267-288.

[21] 李宏男, 成虎, 王东升. 桥梁结构地震易损性研究进展述评[J]. 工程力学, 2018, 35(9): 1-16.

[22] Nielson B G. Analytical fragility curves for highway bridges in moderate seismic zones[D]. Atlanta: Georgia Institute of Technology, 2005.

[23] Porter K, Kennedy R, Bachman R. Creating fragility functions for performance-based earthquake engineering[J]. Earthquake Spectra, 2007, 23(2): 471-489.